

Thepperumal Sampath Kumar^a, Shanmugavel Balasivanandha Prabu^b, Kuraganti Vasu^{c,d}, Mamidipudi Ghanashyam Krishna^c

^aDepartment of Mechanical Engineering, C. Abdul Hakeem College of Engineering and Technology, Melvisharam, Vellore District, India

^bDepartment of Mechanical Engineering, College of Engineering Guindy, Anna University, Chennai, India

^cSchool of Physics, University of Hyderabad, Hyderabad, India

^dPresent Address: Physics and Chemistry of Materials Unit, Jawaharlal Nehru Centre for Advanced Scientific Research, Jakkur, Bangalore, India

Metallurgical characteristics and machining performance of nanostructured TNN-coated tungsten carbide tool

The effect of depositing Nb-rich $Ti_{1-x}Nb_xN$ coatings on the metallurgical characteristics and machining performance of tungsten carbide tools is investigated. The direct current reactive magnetron sputter deposited $Ti_{1-x}Nb_xN$ thin film was crystalline in the as-deposited state. The surface of the film is characterized by a dense granular structure with very few voids and lower roughness than the pristine tungsten carbide surface. Nanoindentation studies revealed that the $Ti_{1-x}Nb_xN$ coating enhanced the hardness and Young's modulus of the tungsten carbide tool to 35 GPa and 703 GPa, respectively, as compared to 20 GPa and 550 GPa respectively, for the uncoated tool. Scratch tests showed that the $Ti_{1-x}Nb_xN$ coating increased the adhesion strength on the tungsten carbide tool. Similarly, the tool wear, surface roughness and cutting force in turning an EN24 alloy steel component displayed significant improvement due to the $Ti_{1-x}Nb_xN$ coating. The minimum surface roughness, minimum tool flank wear and minimum cutting forces were predicted for $Ti_{1-x}Nb_xN$ coated tools based on the Taguchi experimental design.

Keywords: Physical vapour deposition; $Ti_{1-x}Nb_xN$ coating; Metallurgical characteristics; Machinability; Taguchi design

1. Introduction

Hard coatings are important for cutting tool industries to meet the demand of higher production with economy. Physical vapour deposition (PVD) is an extremely reliable technique for the industrial production of coated tools [1, 2]. Cemented carbide tools are commonly used as cutting tools for machining hard materials such as alloy steels and high speed steels [3]. It is known that tool wear is high in cemented carbide tools when machining harder materials. A variety of coatings based on TiN, TiCN, TiC and Al_2O_3 [4] are deposited on cemented carbide cutting tools, in order to improve the hardness of the cutting tool material, thereby reduce the tool wear and improve the surface finish of the

workpiece. Coated cutting tools have shown advantages such as higher wear resistance and lower heat generation, even under extreme cutting conditions. In addition to binary nitrides, ternary compounds that have been used to enhance tool performance include TiAlN, TiCrN, TiSiN and TiNbN coatings, synthesized via PVD, due to their superior mechanical properties and higher wear resistance [5–9]. It has been reported recently that approaches involving multilayers and superlattices of TiN/NbN, TiN/CrN and TiN/VN also exhibit high hardness of the order of 30, 34 and 23.14 GPa respectively, in addition to high wear resistance [10]. Furthermore, the properties and structure of the coatings depend on deposition conditions, such as bias voltage, substrate temperature, reactive gas flow rate, etc., [11]. The experimental and regression model for PVD coated ceramic tools employed in turning of AISI 8660 hardened alloy steel, has shown that the feed rate is the dominant factor in controlling the surface roughness [12].

In earlier work, some of the current authors have shown that the hardness of $Ti_{1-x}Nb_xN$ films can be improved by increasing the Nb content. The Nb rich composition exhibited hardnesses up to 30 GPa as compared to 15 GPa for the base TiN compound [13, 14]. There are no reports on the use of Nb doping in TiN to improve the wear resistance, hardness, adhesive strength, corrosion resistance and surface finish of tungsten carbide tools. Therefore, the objective of the present study is to deposit a nanostructured Nb rich $Ti_{1-x}Nb_xN$ coating (termed as TNN coating in the rest of the paper) on a tungsten carbide insert, using direct current (DC) reactive magnetron sputtering, and investigate its effect on tribological performance and wear resistance of the insert for cutting tool applications.

2. Experimental details

2.1. Deposition of TNN coating on tungsten carbide inserts

The $Ti_{1-x}Nb_xN$ (TNN) films were deposited on the tungsten carbide (WC) insert using DC reactive magnetron sputtering. A base pressure of 3×10^{-6} mbar was achieved in the process chamber in 90 min, using a combination of turbo-

molecular and rotary pumps. After achieving the base pressure, the process chamber is filled with Ar (sputtering gas) and N₂ (reactive gas) to a working pressure of 3.2 × 10⁻² mbar. A circular disc of titanium of 50 mm diameter and 1 mm thickness is used as the cathode (sputtering target). In order to obtain the ternary TNN films, small Nb pieces were placed on the circumference of the region of Ti target erosion [15]. The tungsten carbide inserts were placed at a distance of 40 mm from the target. The sputtering was carried out a power density of 2 W cm⁻² and the substrate temperature was maintained at 250 °C during deposition.

The developed TNN films were characterized for crystal structure using a powder X-ray diffractometer (XRD) (BRUKER D8-Advance, Germany) (X-ray source = Cu-K_α and wavelength of X-ray = 1.5418 Å). The microstructure of the coatings was determined using a high resolution scanning electron microscope (HRSEM) (Quanta FEG 200, Germany) equipped with an energy dispersive X-ray spectrometry (EDX) facility. The coating thickness, determined to be 250 ± 30 nm for a deposition time of 30 min, was measured using a Fisherscope X Ray® X DAL® device and WinFTM software. The hardness of the coatings was determined using a Nanoindenter equipped with a Berkovich indenter (CSM Instruments, Switzerland) with the following parameters: indenter geometry – 120° conical, indenter tip material – diamond, indenter tip radius – 200 µm). The load was increased after the initial contact of the indenter on the surface at a predetermined rate (10 mN min⁻¹) to the desired maximum load (5 mN) and then decreased at the same rate (10 mN min⁻¹) to zero. The hardness and Young's modulus of TNN coating were determined using the Oliver and Pharr method [16] in which the hardness (*H*) is given as

$$H = P_{\max}/A(h_{c(\max)}),$$

where *P*_{max} = peak applied load in newtons, *A*(*h*_{c(max)}) = indenter (probe tip) area calibration function for successive higher loads (*P*_{max}). The TNN coatings on tungsten carbide were subjected to 10 trials for the indentation measurements. The scratch resistance of the coating was tested with a scratch tester (Ducom, V2.1, USA) equipped with a conical shape Rockwell C diamond indenter tip using the C – 1624 – 05 (ASTM) standard. The surface morphology of the coatings was analyzed in an atomic force microscope (AFM, Nanosurf® easyScan 2 controller, Switzerland).

2.2. Machining studies

EN24 alloy steel is used in various applications such as axle shafts, gears and differential shafts in marine environments, connecting rods, aerospace, automobiles and other industrial products such as gears, bolts and studs. Therefore, it was selected as the work piece material for carrying out the turning experiments. Machining studies on the TNN coated inserts were conducted on a solid bar of EN24 alloy steel (90 mm in diameter, 400 mm long and 4.5 GPa hardness) in a conventional lathe machine with dry environment. The turning experiments were planned according to Taguchi's orthogonal array (L₉). A triangular insert (60°) with clearance angle (7°), insert grade (K10) and corner radius (0.8 mm) was used as a cutting tool insert. The total

machining length was taken as 100 mm. The design of experiments for the main factors and levels are shown in Table 1. The L₉ orthogonal array used for the experimental work is shown in Table 2. The objective of the trials was to determine the optimum cutting conditions based on the minimum tool wear, minimum cutting forces and minimum surface roughness from the output values. The flank tool wear was measured using a tool maker's microscope and the surface roughness was measured by using a mahr surface roughness tester (Marsurf GD 120). Machining forces such as feed force (*F*_x), thrust force (*F*_y) and cutting force (*F*_z) were measured by using a tool Kistler® dynamometer with the help of DynoWare software. The cutting parameters are analyzed using Minitab 15 software for both tool wear and surface roughness.

3. Results and discussion

3.1. Microstructural and compositional analysis

A cross-sectional SEM image of the TNN coating on the WC insert is shown in Fig. 1a. The interface between the tungsten carbide and TNN coating can be clearly distinguished from the different microstructural features. The magnified views of the TNN-coated surface of tungsten carbide in Fig. 1b and c show that it is composed of 1–5 µm sized crystals. The surface shows a dense morphology and uniform grain structure with very few pores [17, 18]. It is seen that the surface of the TNN coating is smoother than that of the tungsten carbide insert. The line scan performed to obtain the EDX spectrum along with the elemental com-

Table 1. Design of experiment for the main factors and levels.

Main factors	Levels		
	1	2	3
Cutting speed (m min ⁻¹)	V1 = 40	V2 = 100	V3 = 160
Feed rate (mm rev ⁻¹)	f1 = 0.119	f2 = 0.318	f3 = 0.477
Depth of cut (mm)	d1 = 0.3	d2 = 0.7	d3 = 1.0

Table 2. L₉ orthogonal array.

Experiment trials	Cutting speed (m min ⁻¹)	Feed rate (mm rev ⁻¹)	Depth of cut (mm)
L1	V1	f1	d1
L2	V1	f2	d2
L3	V1	f3	d3
L4	V2	f1	d2
L5	V2	f2	d3
L6	V2	f3	d1
L7	V3	f1	d3
L8	V3	f2	d1
L9	V3	f3	d2

position of the TNN coating are shown in Fig. 1d and table in the inset, respectively. It shows that the coating is an Nb-rich $Ti_{1-x}Nb_xN$ composition with 55 at.% of Nb compared to 11 at.% of Ti.

3.2. Structural analysis

The XRD pattern of the TNN coating is shown in Fig. 2a, in which the peak at 35.99° corresponds to TNN. The formation of the TNN phase is further confirmed using the selected area electron diffraction (SAED) pattern shown in Fig. 2b which shows concentric rings that correspond to (111), (200) and (202) planes of $Ti_{1-x}Nb_xN$ in conformity with results previously reported by some of the current authors [13, 14]. A comparison with standard JCPDS files indicates that the higher angle XRD peaks in the 2θ range from 65° to 120° can correspond to TiN, NbN or Ti_4Nb . The diffraction peak at 74.40° can be assigned to both TiN (311) and NbN (222) planes due to the strong overlap. The peak at 109.10° is indexed as belonging to the (307) plane of NbN whereas the peak at 99.79° can be assigned to the (331) plane of NbN or the (311) plane of Ti_4Nb . Since the deposition is carried out in an atmosphere of argon and nitrogen, the possibility of the formation of Ti_4Nb is very low and hence this peak is assigned to NbN. Two significant observations can be made from the XRD patterns: (1) The sharp peaks indicate a high degree of crystallinity and (2) The presence of peaks from TiN and NbN indicate the composite nature of the TNN coating (i.e. it is a composite of TNN, TiN and NbN). An exact determination of the crystallite size is difficult due to the composite nature of the film. However, accounting for the instrumental and strain related broadening it can be stated qualitatively that the film is nanocrystalline in nature [19–24].

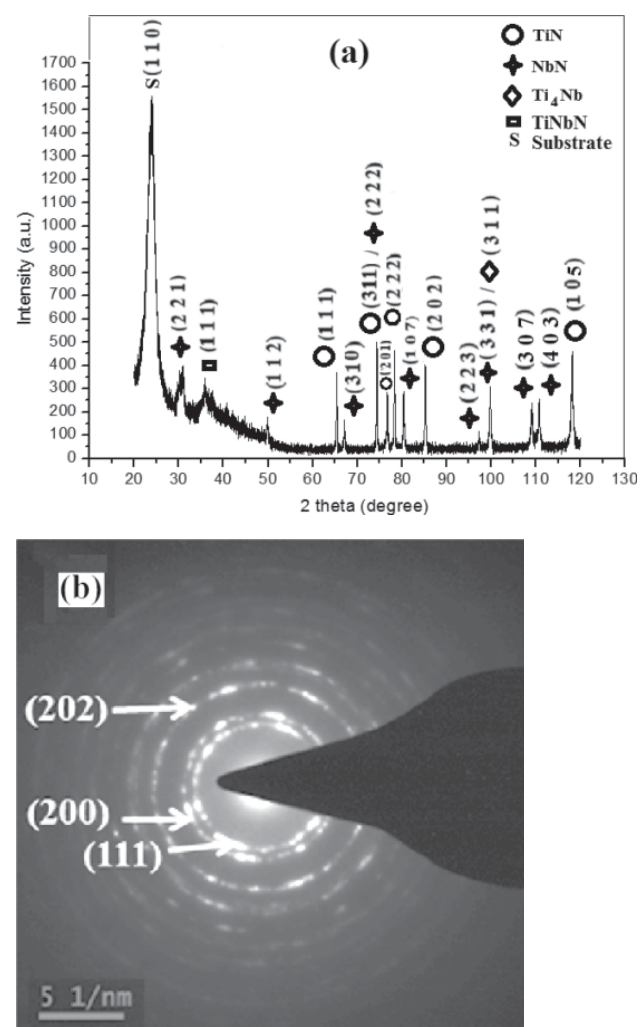


Fig. 2. (a) X-ray diffraction of TNN coating and (b) SAED pattern of TNN coating.

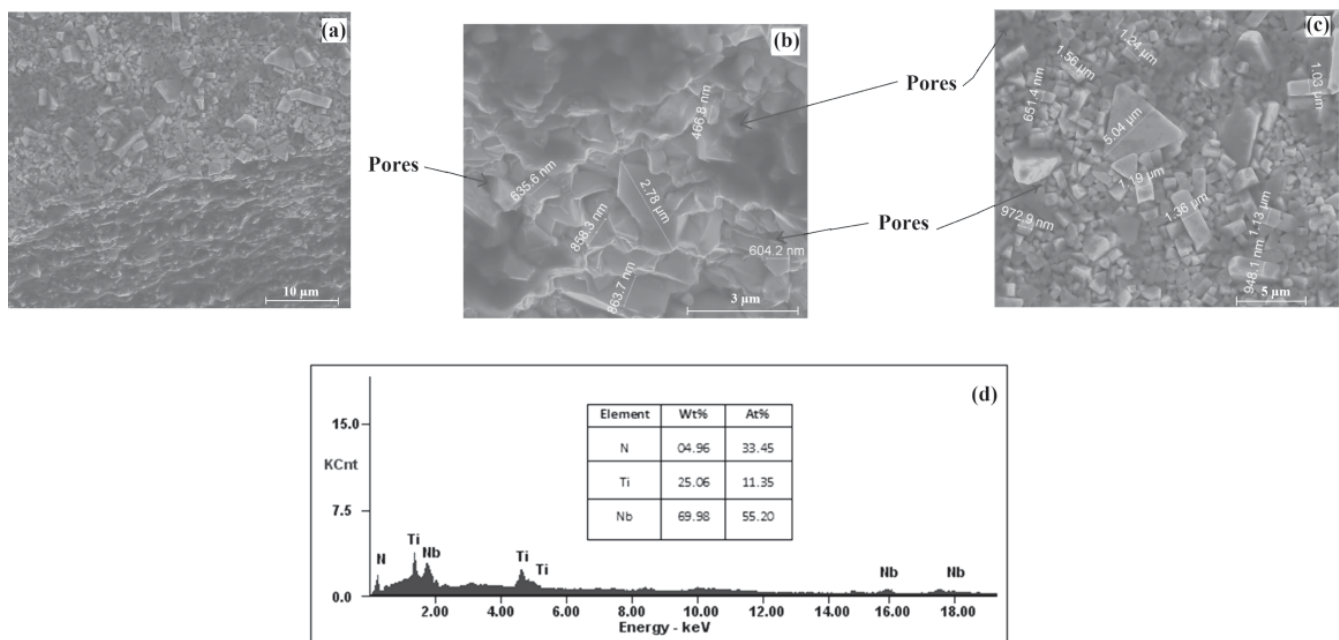


Fig. 1. (a) Cross-sectional SEM image of $Ti_{1-x}Nb_xN$ coating on tungsten carbide, (b) and (c) magnified views of top surface of $Ti_{1-x}Nb_xN$ coating on tungsten carbide substrate showing formation of faceted crystals (d) EDX spectrum and elemental composition of the $Ti_{1-x}Nb_xN$ coating on tungsten carbide.

3.3. Nanoindentation

The load vs displacement curve during nanoindentation on TNN coating is shown in Fig. 3 and a summary of the results obtained is presented in Table 3. Since the indentation depth is > 10 % of the film thickness, the value corresponds to that of film + substrate and not the “film-only” hardness. The results clearly indicate that the TNN coating has higher hardness than other coatings such as TiN/NbN, TiN/CrN and TiN/VN with hardnesses of 30, 34 and 23.14 GPa respectively. The value of H^3/E^{*2} (0.076 GPa) indicates resistance to plastic deformation. This value is lower than the value reported by Musil et al. for Cr–Ni–N films [25]. This shows the developed coating is a hard coating with high plastic deformation ability. However, on comparing the hardness of the substrate, the coating shows improved

hardness and Young’s modulus. Furthermore, elastic recovery (W_e) is low and plastic recovery (W_p) is high for the TNN coated insert leading to higher Young’s modulus. The composite hardness is 35.7 GPa with a Young’s modulus of 703 GPa. A comparison with the values obtained for the uncoated tool (hardness = 20 GPa and Young’s modulus = 550 GPa) shows that the composite hardness is much higher and comparable with literature values on WC tool inserts coated with nitride thin films [26].

3.4. Scratch test analysis

The adhesion strength of the TNN coating along with the different loading conditions and other testing parameters for scratch testing are listed in Table 4. The traction force vs stroke curves and the optical image of the scratched region is shown in Fig. 4. In the constant load test, each scratch track is associated with a specific constant stylus normal force. This normal force acts as the critical load (L_{CN}) at which failure for a given scratch track occurs, as it is constant over the entire length of the scratch [27]. The traction force and co-efficient of friction (μ) are affected by changes in the surface roughness along the scratch track, in the stylus drag and stress. Failure modes of the TNN coating for the progressive load scratch test are presented in Table 5. The values of the failure mode (N) are calculated using Eq. (1). The critical load for the progressive type can be calculated using:

$$L_{CN} = (L_{rate}(I_N/X_{rate})) + L_{start} \quad (1)$$

where,

L_{rate} – The rate of force application ($N \text{ min}^{-1}$) in the specific scratch test

I_N – The distance in mm between the start of the scratch track and the start point of the defined type of damage in the scratch track

X_{rate} – The rate of horizontal displacement (mm min^{-1}) in the specific scratch test

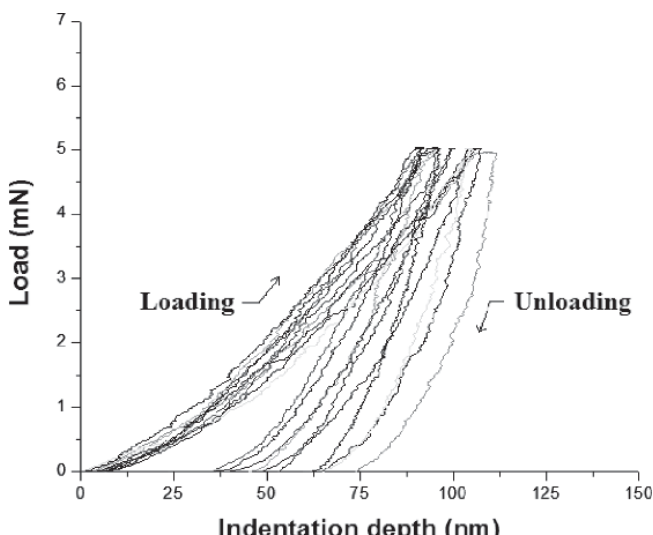


Fig. 3. The load vs displacement curves of TNN coating.

Table 3. Mechanical properties of TNN coatings measured at a load of 5 mN.

Sl. No	Coating	H (GPa)	HV (Vickers)	E (GPa)	E^* (GPa)	W_e (%)	W_p (%)	H^3/E^{*2} (GPa)
1.	TNN	35.67	3303.73	703.12	772.66	43.97	56.02	0.076

Table 4. Scratch test parameters.

Sl.No	Parameters	Details
1.	Constant load (individual scratches)	20 N, 30 N, 40 N, 50 N
2.	Progressive load (ramp load)	20 N (initial) to 50 N (final)
3.	Incremental load rate for progressive	10 N mm^{-1}
4.	Loading rate	300 N min^{-1}
5.	Scratch length	3 mm
6.	Scratch speed	30 mm min^{-1}
7.	Indenter geometry	120° Conical
8.	Indenter material (tip)	Diamond
9.	Indenter tip radius	200 μm

L_{start} – The preload stylus force (Newtons) established at the start of the scratch test

It is evident that the adhesion strength is high for the TNN-coated WC insert. The TNN coating was first subjected to cohesive failure (chipping). As a consequence, wedging spallation or spalling of the coating which is followed by further adhesive failure in the coating (spallation or interface failure) occurs in the scratch track. The coating delaminated and total failure occurred when the scratch time was further increased [28]. The high bonding strength (adhesive strength) and high scratch resistance of the TNN coated tool is due to the presence of Nb which causes segregation of TNN in to a nanocrystalline composite of TNN, TiN and NbN and the uniform dispersion of nano-crystallites.

3.5. Surface analysis

3D and 2D atomic force microscopy images of the TNN coating, where the Z range varies from $2 \mu\text{m}$ to $22 \mu\text{m}$, are shown in Fig. 5a and b. The average surface roughness of TNN was measured as 9.3 nm , which is much lower than conventional coatings such as TiAlN and AlCrN [29, 30] used for similar applications. The texture misorientation of

the grains/droplets is a consequence of the rough surface. The TNN coating has particle sizes which vary from 250 nm to 900 nm . A summary of surface roughness values of TNN film from AFM analysis is presented in Table 6.

3.6. Cutting force analysis

Machining studies on an EN24 alloy steel component were performed using the TNN coated tool. The cutting forces obtained under different machining conditions are presented in Table 7. In the various trial conditions used, minimum machining forces were recorded in the L8 trial condition for the TNN coated tool. The optimal cutting condition for L8 is $V = 160 \text{ m min}^{-1}$, $f = 0.318 \text{ mm rev}^{-1}$ and $d = 0.3 \text{ mm}$. The machining forces $F_x = 3.566 \text{ N}$, $F_y = 24.47 \text{ N}$ and $F_z = 29.13 \text{ N}$ are recorded as the lowest forces during machining. The highest machining force is obtained in L5 trial. The low machining forces and lower tool wear observed in the TNN coating indicate that L8 is the optimal cutting condition. The surface roughness values are also lower for the TNN coating in the L8 trial. In contrast, for the uncoated tool, minimum machining forces were obtained for the L1 trial condition. The optimal cutting condition for L1 is $V = 40 \text{ m min}^{-1}$, $f = 0.119 \text{ mm rev}^{-1}$ and $d = 0.3 \text{ mm}$ and the minimum cutting forces were $F_x =$

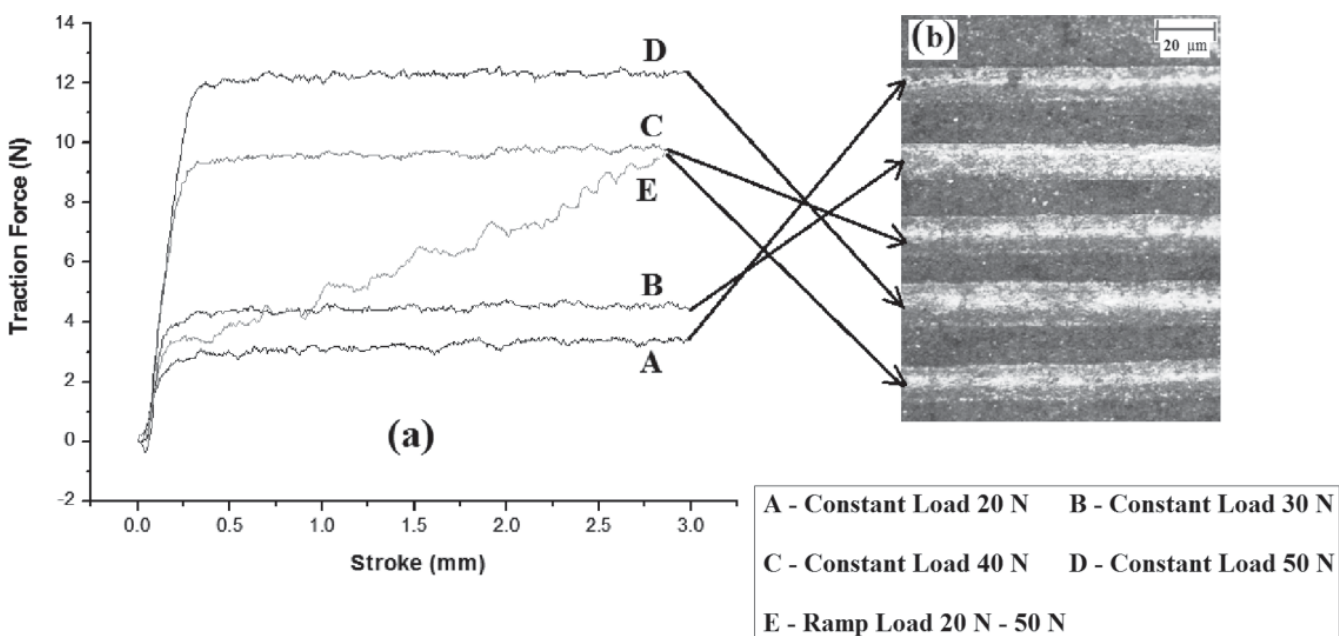


Fig. 4. (a) Traction force vs stroke curves recorded during a scratch test of the TNN coating, (b) Optical microscopy images of constant load and progressive load scratch tracks.

Table 5. Failure mode results for the progressive load scratch test.

Sl. No	Substrate	Coating	Failure mode (N)			
			L_{C1}	L_{C2}	L_{C3}	L_{C4}
1.	Cemented carbide	TNN	26	41	42.2	46.8

L_{C1} – Coating crack (cohesive failure); L_{C2} – Adhesive chipping at crack edges (adhesive failure); L_{C3} – Initial failure of the coating; L_{C4} – Total failure of the coating.

20.84 N, $F_y = 47.23$ N and $F_z = 77.81$ N. Furthermore, the highest machining force obtained for the uncoated tool was achieved in the L3 trial ($V = 40$ m min $^{-1}$, $f = 0.477$ mm rev $^{-1}$ and $d = 1.0$ mm). High machining forces cause inaccuracy and instability in tools which are subjected to pressure and opposing stresses during cutting. Cutting forces are used to find the energy consumption and machining power requirements. In hard turnings, higher cutting forces are obtained while machining a hard material, which reduces the performance of the cutting tool [31, 32].

3.7. Surface roughness analysis

The surface roughness value of 1.537 μm recorded for the TNN coated tool was much lower than the 2.308 μm for the uncoated tool, as presented in Table 8. The optimum surface roughness for the TNN coated tool was observed in the L8 trial. The optimal cutting condition for L8 is $V = 160$ m min $^{-1}$, $f = 0.318$ mm rev $^{-1}$ and $d = 0.3$ mm. The optimum surface roughness for the uncoated tool was achieved during the L5 trial, wherein the optimal cutting conditions are $V = 100$ m min $^{-1}$, $f = 0.318$ mm rev $^{-1}$ and

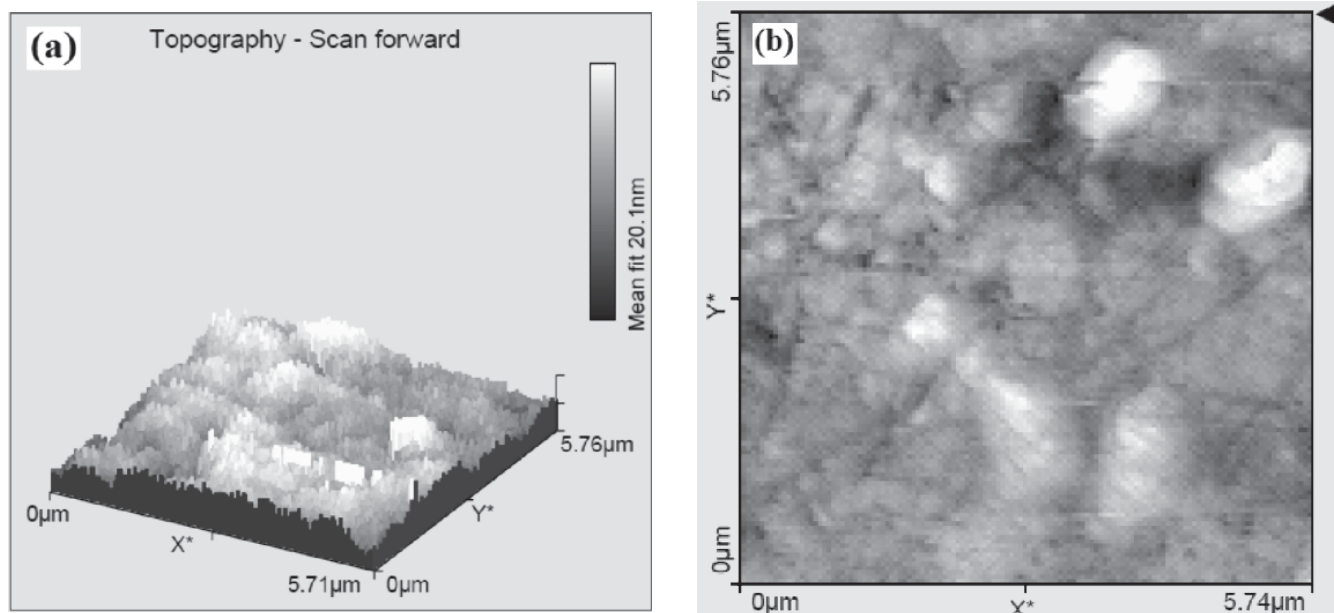


Fig. 5. (a) 3D and (b) 2D AFM images of TNN-coated tool.

Table 6. Surface roughness values for the TNN coating.

Sl. No	Coating	S_a (nm)	S_q (nm)	S_y (nm)	S_p (nm)	S_v (nm)	S_m (nm)
1.	TNN	9.3	13	120	76	-45	0.22

S_a – Roughness value, S_q – Root mean square, S_y – Peak to valley height ($S_p - S_v$), S_p – Peak height, S_v – Valley depth, S_m – Mean value

Table 7. Various machining forces obtained for the TNN-coated tools and uncoated carbide tools.

Experiment trials	Various machining forces for TNN-coated tools (N)			Various machining forces for uncoated tools (N)		
	Feed force (F_x)	Thrust force (F_y)	Cutting force (F_z)	Feed force (F_x)	Thrust force (F_y)	Cutting force (F_z)
L1	11.76	93.37	149.92	20.84	47.23	77.81
L2	107.09	152.70	312.89	120.70	268.00	357.20
L3	87.08	101.65	196.73	233.10	552.90	690.70
L4	30.93	69.47	92.97	137.00	160.10	208.60
L5	113.03	254.05	433.48	206.60	332.40	449.90
L6	13.48	65.35	82.19	55.49	248.80	255.70
L7	81.36	180.87	279.84	142.90	189.80	224.10
L8	3.56	24.47	29.13	42.53	168.60	156.50
L9	31.86	140.80	213.30	122.70	373.50	407.50

$d = 1.0$ mm. The surface roughness values increase gradually at low cutting speed, when the feed rate increases [33, 34]. At higher cutting speeds and feed rates, the surface roughness decreases and then increases, when the depth of cut is low. The ANOVA for the surface roughness and percentage contributions of the cutting parameters of TNN coated and uncoated tools are shown in Table 9. The cutting speed has a high percentage contribution, followed by the feed rate and the depth of cut for the TNN coated cutting tool. In contrast, for the uncoated cutting tool, feed rate has the highest percentage contribution followed by cutting speed and depth of cut.

3.8. Tool wear analysis

The tool flank wear vs the length of cut, in Fig. 6, shows that the minimum flank tool wear measured for the TNN coated tool was 0.06 mm, which is lower than that for the uncoated tool at 0.09 mm. The optimum tool wear for the TNN coated tool was observed when $V = 160$ m min $^{-1}$, $f = 0.318$ mm rev $^{-1}$ and $d = 0.3$ mm. The tool wear occurred due to the high temperature and stresses during cutting, which cause the cutting edges to thermally soften and degrade. This, in turn, causes the cutting edges to become blunt resulting in the occurrence of built-up-edge (BUE)

which adhered to the tool during chip movement. For the TNN-coated tools, excluding the L1 experimental trial, BUE is observed in all trials from L2 to L9. In comparison, for the uncoated tool BUE is evident in all the experimental

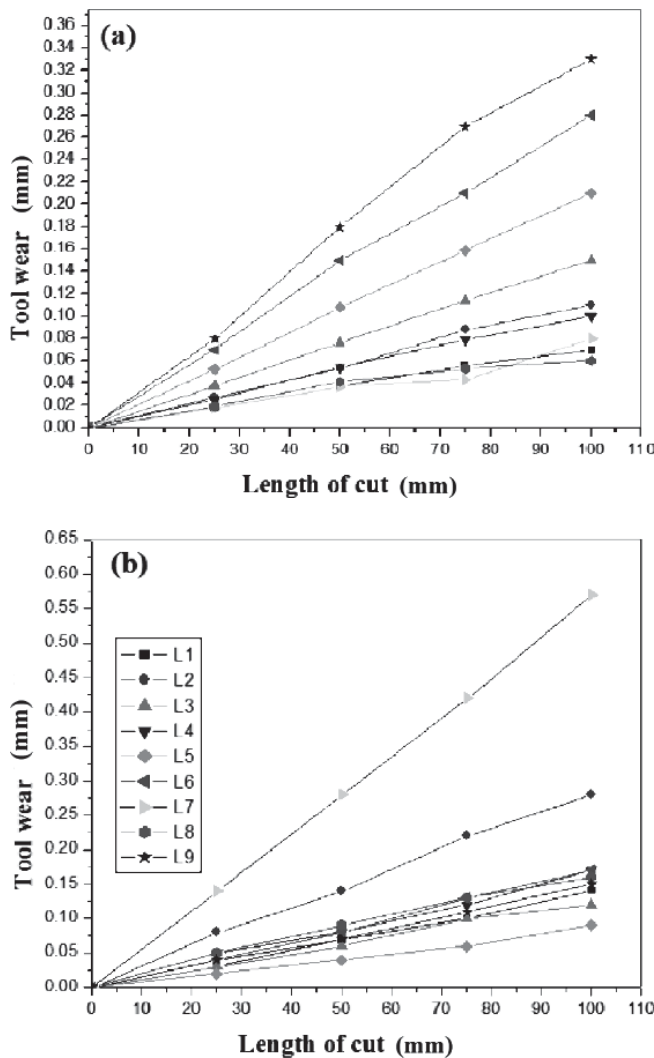


Fig. 6. Progression of flank wear for (a) TNN-coated tools (b) Uncoated tools.

Table 8. Surface roughness values for the TNN-coated tools and uncoated carbide tools.

Experiment trials	Surface roughness values (μm)	
	TNN coated tool	Uncoated tool
L1	2.545	3.466
L2	3.602	3.747
L3	4.257	5.874
L4	2.946	3.122
L5	2.250	2.308
L6	3.408	4.108
L7	1.843	2.440
L8	1.537	2.811
L9	2.884	3.828

Table 9. Results of the ANOVA for the surface roughness of workpiece of TNN-coated and uncoated tools.

Cutting parameter	Degree of freedom	Sum of squares	Mean square	F ratio	Contribution (%)
a) TNN					
Cutting speed	2	30.90343	15.45171	6.583623	48.78239
Feed rate	2	25.86981	12.9349	5.511268	40.83661
Depth of cut	2	1.882331	0.941166	0.401009	2.971341
Error	2	4.693985	2.346992		7.409657
Total	8	63.34955			100
b) Uncoated					
Cutting speed	2	17.17022	8.58511	14.56337	34.37071
Feed rate	2	28.14287	14.07144	23.87011	56.33535
Depth of cut	2	3.463879	1.73194	2.937979	6.933864
Error	2	1.179	0.5895		2.360079
Total	8	49.95597			100

trials. The optical images of flank tool wear recorded for TNN-coated tools and uncoated tools, respectively, are shown in Fig. 7. The coated tool reduces the friction at the chip–tool interface; therefore the cutting force and power were reduced considerably. The coated tool improves the surface quality and reduces BUE formation [35, 36]. The formation of BUE increases the cutting forces and significantly affects the surface finish of the machined workpiece. The ANOVA for the tool wear and various percentage contributions of the cutting parameters for TNN-coated and un-

coated tools are shown in Table 10. In the case of TNN-coated tool, feed rate has the highest percentage contribution followed by cutting speed and depth of cut. However, for the uncoated tool the order of contribution is depth of cut followed by cutting speed and feed rate. SEM images of the rake and flank faces of maximum worn-out TNN coated and uncoated inserts are shown in Fig. 8. From the SEM images, it is evident that the tool wear is higher in uncoated tools with BUE, when compared to the TNN coated tools.

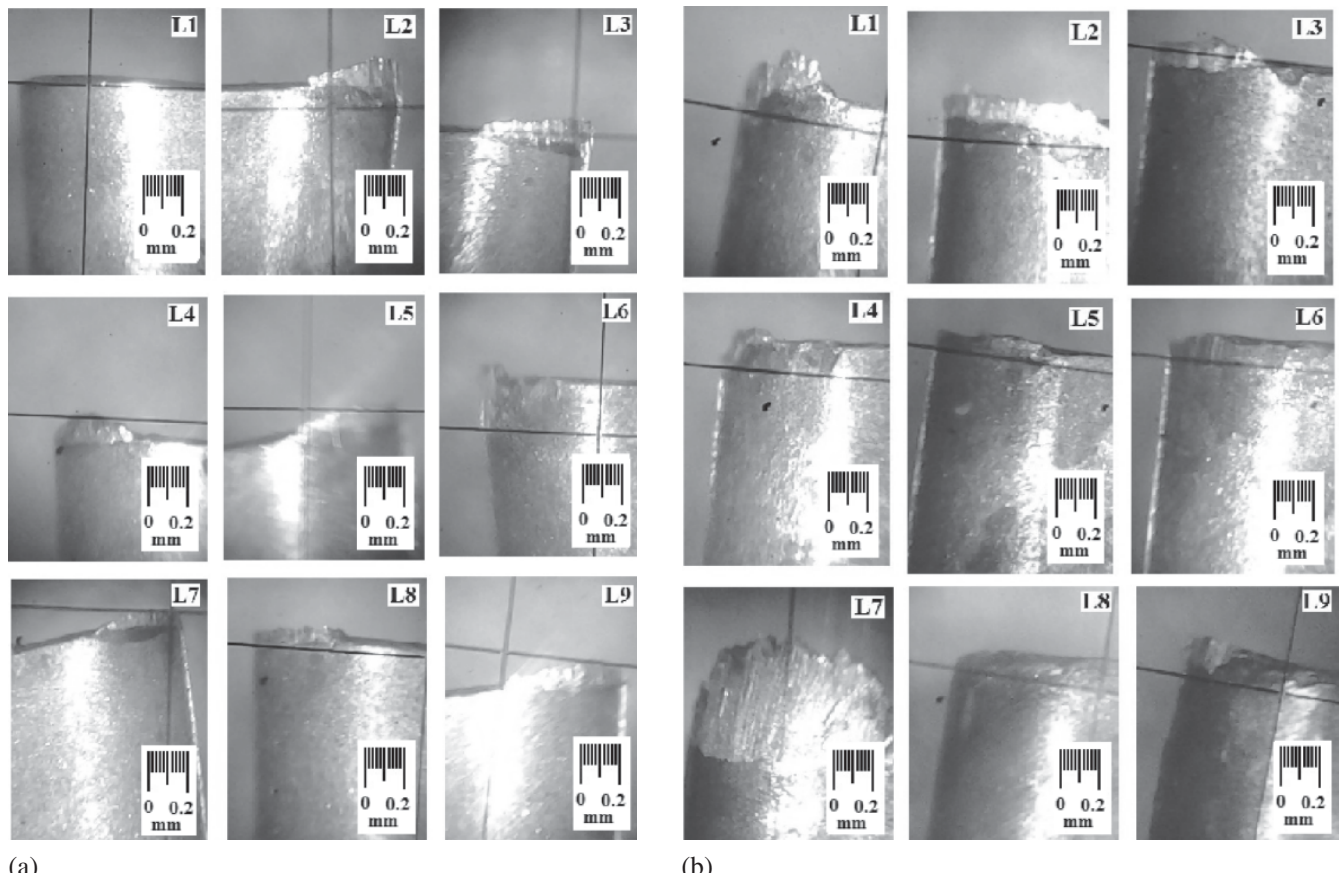


Fig. 7. Optical images of tool flank wear obtained for experimental trials (a) TNN-coated tools (b) Uncoated tools.

Table 10. Results of the ANOVA for tool wear of TNN-coated and uncoated tools.

Cutting parameter	Degree of freedom	Sum of squares	Mean square	F ratio	Contribution (%)
a) TNN					
Cutting speed	2	37.4598	18.7299	2.25185	16.43879
Feed rate	2	137.6424	68.82118	8.274202	60.40271
Depth of cut	2	36.13722	18.06861	2.172345	15.85839
Error	2	16.63512	8.317561		7.300124
Total	8	227.8745			100
b) Uncoated					
Cutting speed	2	35.59655	17.79827	6.55464	20.67275
Feed rate	2	31.56749	15.78375	5.812742	18.33287
Depth of cut	2	99.59588	49.79794	18.33928	57.84047
Error	2	5.43074	2.71537		3.153911
Total	8	172.1907			100

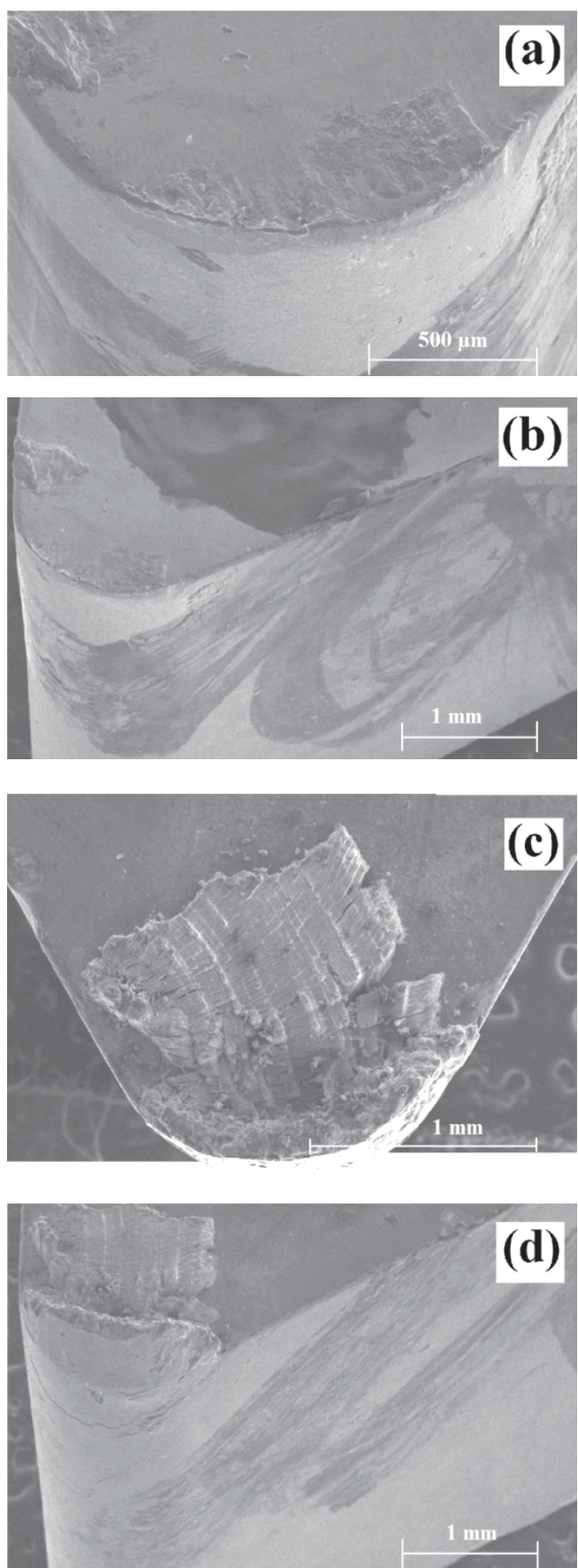


Fig. 8. SEM images of worn-out coated and uncoated cutting tool inserts (a) Rake face of TNN-coated insert (b) Flank face of TNN-coated insert (c) Rake face of uncoated insert (d) Flank face of uncoated insert.

3.9. Chip formation analysis

The images of chip formation obtained from experimental trials are shown in Fig. 9a and b for TNN-coated tools and uncoated tools, respectively. Helical chips that can be attributed to the thermal softening and plastic deformation were observed in L5 and L7 trials. However, curved chips were observed in L1, L6 and L9 trials. Curved chips develop due to the thermal softening and instability in the tool

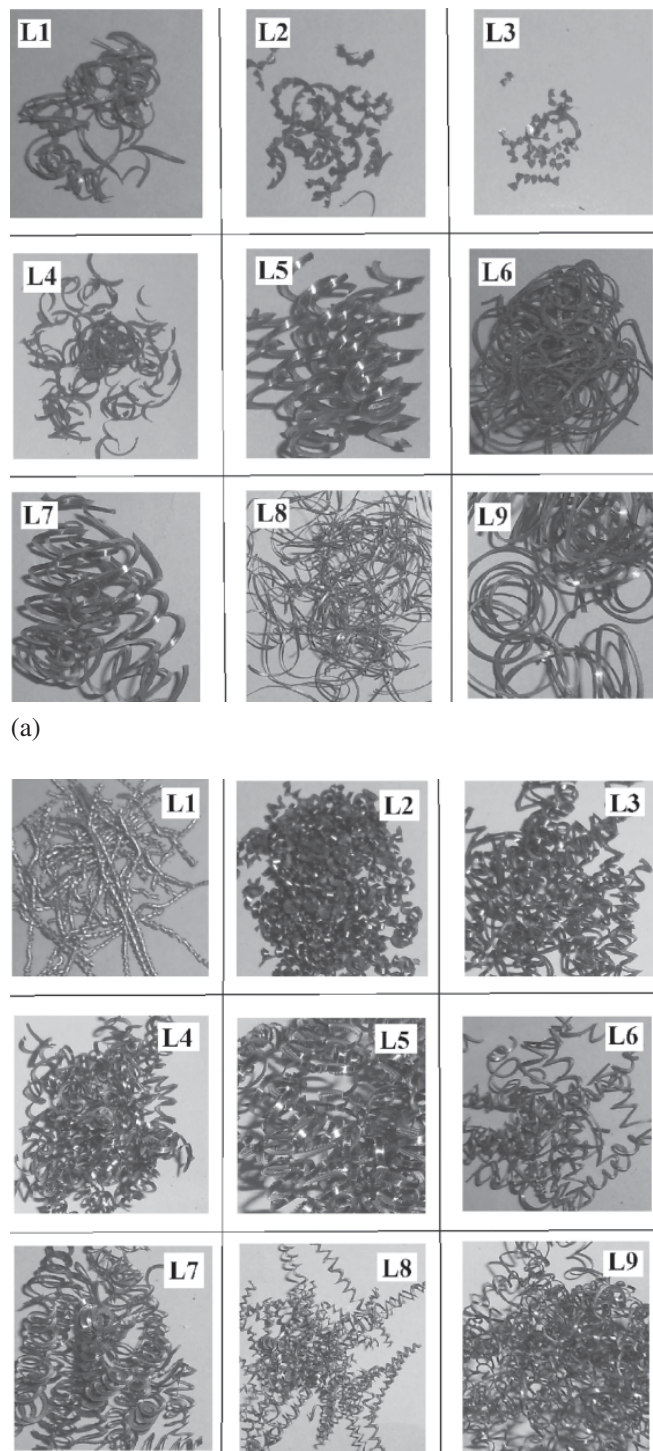


Fig. 9. Various chip shapes of the EN-24 steel for L₉ orthogonal array trials (a) TNN-coated tools (b) Uncoated tools.

edge resulting from high temperature in the cutting zone. The L2 ($V = 40 \text{ m min}^{-1}$, $f = 0.318 \text{ mm rev}^{-1}$ and $d = 0.7 \text{ mm}$) trial produced curved, sharp segmented edges (serrated chips or wavy chips) with breakup chips. These are also known as saw tooth chips, characterized by continuous cyclic segments with uniformly spaced sharp points along the outer surface due to the gradual wearing of the tool. In general, serrated chips are formed if the temperature increases in the primary shear zone. Shear deformation weakens the material by thermal softening and therefore the de-

formation is concentrated in shear bands [37, 38]. The L3 trial ($V = 40 \text{ m min}^{-1}$, $f = 0.477 \text{ mm rev}^{-1}$ and $d = 1.0 \text{ mm}$) resulted in sharp-edged breakup chips, whereas a continuous, thin, curved type of chip was produced in L8 trial ($V = 160 \text{ m min}^{-1}$, $f = 0.318 \text{ mm rev}^{-1}$ and $d = 0.3 \text{ mm}$). This chip is formed due to increase in ductility of the work-piece material, because of high cutting temperature as a consequence of high machining speed. The L4 trial ($V = 100 \text{ m min}^{-1}$, $f = 0.119 \text{ mm rev}^{-1}$ and $d = 0.7 \text{ mm}$) resulted in curved C-type of chips with sharp edges. In con-

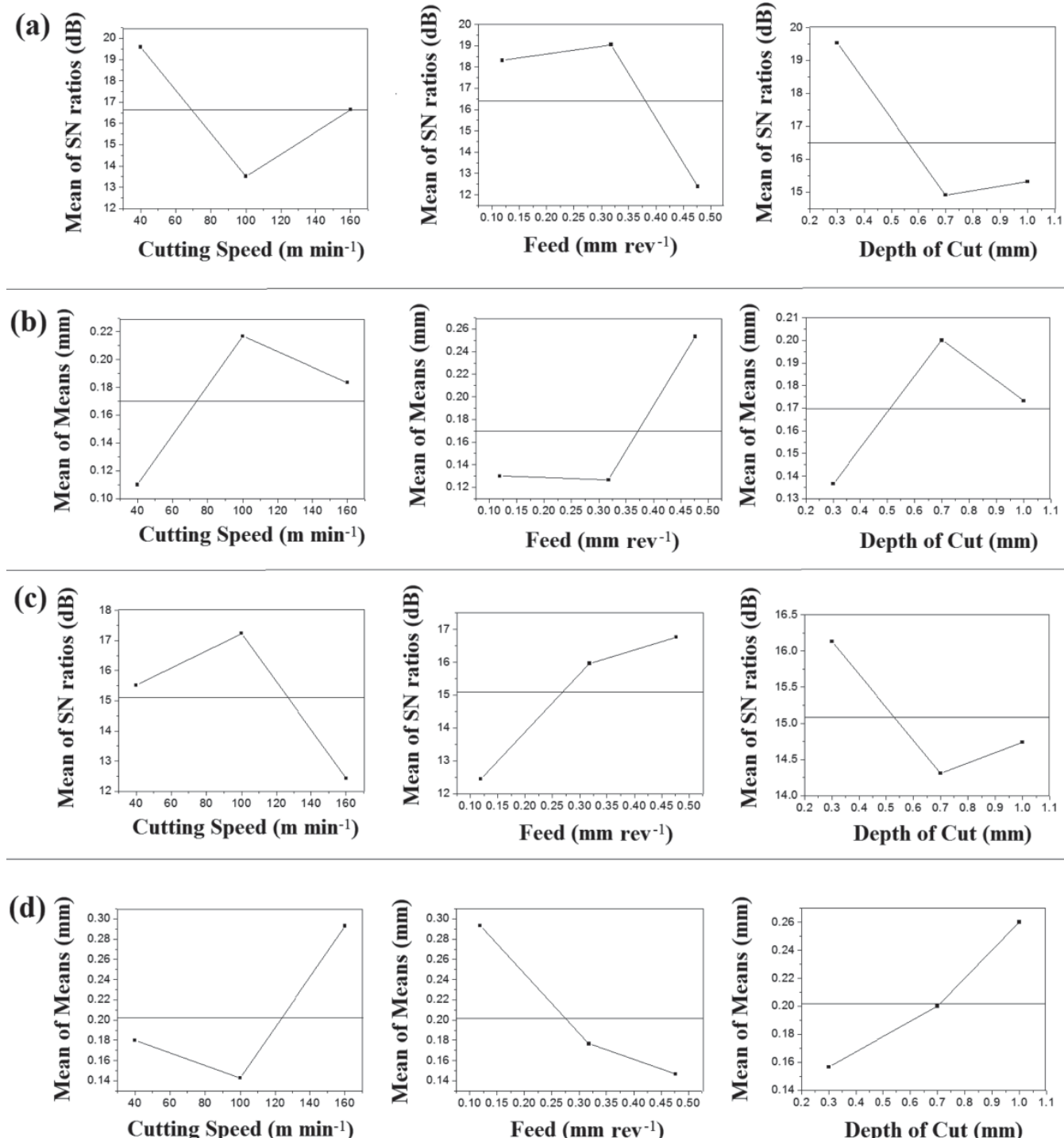


Fig. 10. Main effect plots for coated and uncoated tool wear of S/N ratio and mean graphs. (a) S/N ratio for TNN-coated tool (b) Mean for TNN-coated tool, (c) S/N ratio for uncoated tool (d) Mean for uncoated tool.

trast, the uncoated tool showed small spiral continuous chips in L1 and L8 trials, discontinuous spiral curved chips in the L2 trial, helical continuous chips in the L3 (ie. V1 f3 d3), L4 and L9 trials, ribbon curved chips with one edge saw tooth in the L5 trial and long helical curved chips were obtained in the L6 and L7 trials.

3.10. Taguchi design analysis

Taguchi design analysis was performed on the uncoated and TNN-coated tools. In this analysis, the process parame-

ters with the highest signal to noise (*S/N*) ratio give the optimum quality with minimum variance [39, 40]. The main effect plots, for *S/N* and mean in the case of TNN-coated tool, are shown in Fig. 10a and b, respectively. The corresponding plots for the work piece surface roughness with uncoated and TNN-coated tools are shown in Fig. 11a and b, respectively. The responsible factors for the cutting parameters based on the *S/N* ratios, and the confirmation experimental results for the tool wear and the surface roughness of the work piece are shown in Tables 11 and 12 respectively.

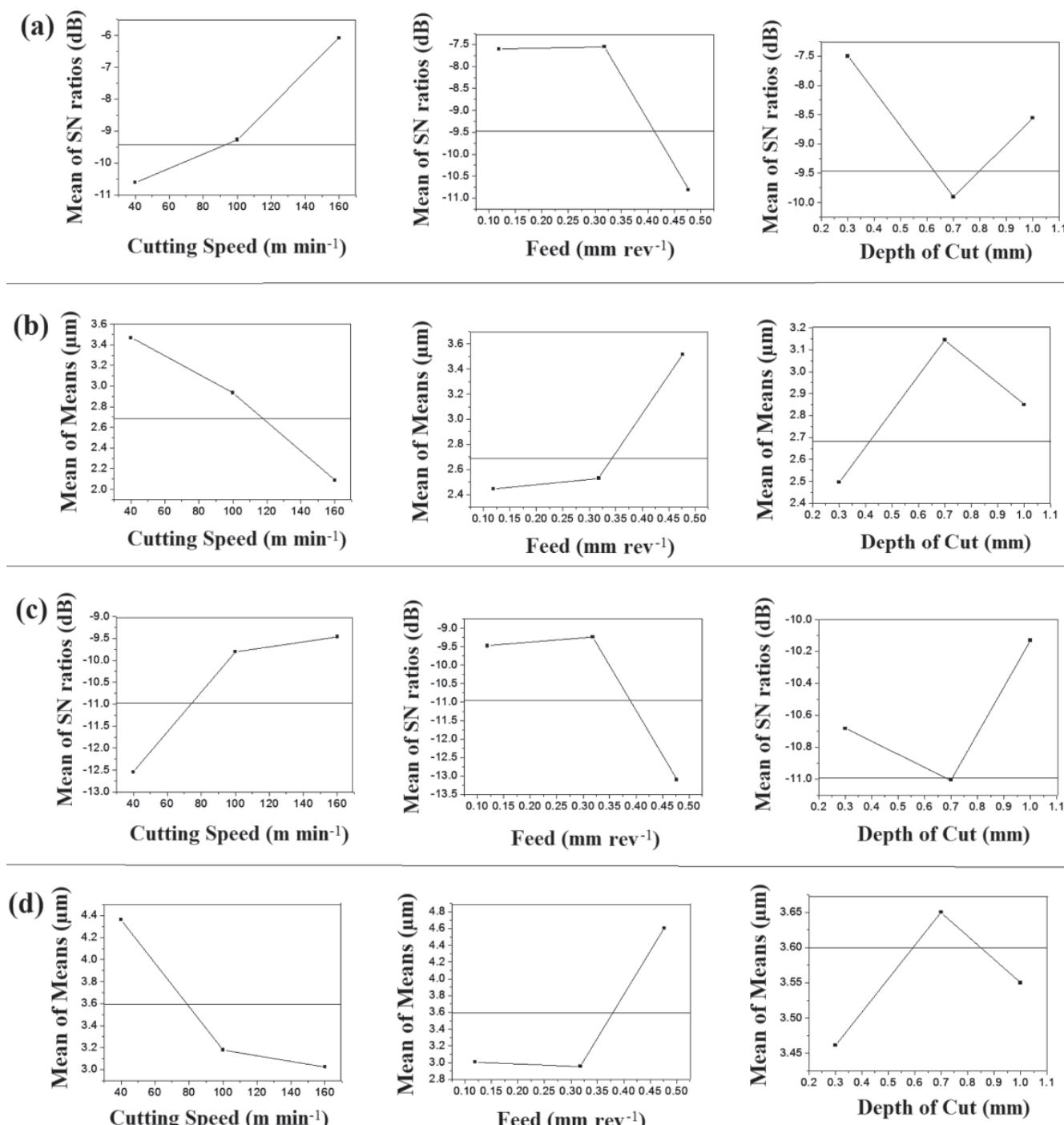


Fig. 11. Main effect plots for the surface roughness of the workpiece in coated and uncoated tools of *S/N* ratio and mean graphs (a) *S/N* ratio for TNN-coated tool (b) Mean for TNN-coated tool, (c) *S/N* ratio for uncoated tool (d) Mean for uncoated tool.

Table 11. Various responsible factors based on the S/N ratio and the confirmation experimental results for the tool wear.

Tool wear						
Coating/ Uncoated	Highly responsible factor	Moderately responsible factor	Least responsible factor	Predicted optimal levels	Predicted value (mm)	Confirmation experiment value (mm)
TNN Uncoated	Feed rate Cutting speed	Cutting speed Feed rate	Depth of cut Depth of cut	V1 f2 d1 V3 f1 d1	0.057 0.280	0.065 0.285

Table 12. Various responsible factors based on the S/N ratio and the confirmation experimental results for the surface roughness.

Surface roughness						
Coating/ Uncoated	Highly responsible factor	Moderately responsible factor	Least responsible factor	Predicated optimal levels	Prediction values (μm)	Confirmation experiment values (μm)
TNN Uncoated	Cutting Speed Feed rate	Feed rate Cutting Speed	Depth of cut Depth of cut	V3 f2 d1 V3 f2 d3	1.550 2.403	1.950 2.953

4. Conclusions

The deposition of Nb rich $\text{Ti}_{1-x}\text{Nb}_x\text{N}$ (TNN) coating on tungsten carbide tools by means of DC reactive magnetron sputtering is demonstrated. The hardness, Young's modulus and all parameters related to machinability such as scratch resistance, tool wear, surface roughness, chip formation and cutting force showed significant improvement due to the TNN coating on the tungsten carbide tool. Thus, the mechanical behaviour of WC tools can be significantly improved by depositing TNN coatings using a cost-effective DC magnetron sputtering process. The best cutting condition is obtained when $V = 160 \text{ m min}^{-1}$, $f = 0.318 \text{ mm rev}^{-1}$ and $d = 0.3 \text{ mm}$, which resulted in better surface finish, minimum tool wear and minimum machining forces.

References

- [1] S. Veprek, J.G.M. Veprek-Heijman: Surf. Coat. Technol. 202 (2008) 5063. DOI:10.1016/j.surfcoat.2008.05.038
- [2] M. Nose, Y. Deguchi, T. Mae, E. Honbo, T. Nagae, K. Nogi: Surf. Coat. Technol. 174–175 (2003) 261.
- [3] A.K. Sahoo, B. Sahoo: Int. J. Ind. Eng. Comput. 2 (2011) 819.
- [4] Z. Hao, D. Gao, Y. Fan, R. Han: Int. J. Mach. Tools Manuf. 51 (2011) 973. DOI:10.1016/j.ijmachtools.2011.08.018
- [5] G.S. Fox-Rabinovich, K. Yamamoto, M.H. Aguirre, D.G. Cahill, S.C. Veldhuis, A. Biksa, G. Dosbaeva, L.S. Shuster: Surf. Coat. Technol. 204 (2010) 2465. DOI:10.1016/j.surfcoat.2010.01.024
- [6] H.C. Barshilia, M. Ghosh, S.R. Ramakrishna, K.S. Rajam: Appl. Surf. Sci. 256 (2010) 6420. DOI:10.1016/j.apsusc.2010.04.028
- [7] S. Boelens, H. Veltrop: Surf. Coat. Technol. 33 (1987) 63. DOI:10.1016/0257-8972(87)90177-0
- [8] I. Grimberg, V.M. Zhitomirsky, R.L. Boxman, S. Goldsmith, B.Z. Weiss: Surf. Coat. Technol. 108–109 (1998) 154.
- [9] A.P. Serro, C. Completo, R. Colaço, F. dos Santos, C. Lobato da Silva, J.M.S. Cabral, H. Araújo, E. Pires, B. Sarramago: Surf. Coat. Technol. 203 (2009) 3701. DOI:10.1016/j.surfcoat.2009.06.010
- [10] C.J. Tavares, L. Rebouta, E. Alves, A. Cavaleiro, P. Goudeau, J.P. Riviere, A. Declémé: Thin Solid Films 377–378 (2000) 425.
- [11] B. Window: Surf. Coat. Technol. 81 (1996) 92. DOI:10.1016/0257-8972(95)02620-7
- [12] A.R. Motorcu: J. Mech. Eng. 56 (6) (2010) 391.
- [13] K. Vasu, M. Ghanashyam Krishna, K.A. Padmanabhan: J. Mater. Sci. 47 (2012) 3522. DOI:10.1007/s10853-011-6197-x
- [14] K. Vasu, M. Ghanashyam Krishna, K.A. Padmanabhan: AIP Conf. Proc. 1451 (2012) 239.
- [15] N.H. Shah, T. Jayaganthan, D. Kaur, R. Chandra: Thin Solid Films 518 (2010) 5762. DOI:10.1016/j.tsf.2010.05.095
- [16] A.C. Fischer-Cripps: Surf. Coat. Technol. 200 (2006) 4153. DOI:10.1016/j.surfcoat.2005.03.018
- [17] H.C. Barshilia, B. Deepthi, N.S. Kumar, A. Jain, K.S. Rajam: Appl. Surf. Sci. 253 (2007) 5076. DOI:10.1016/j.apsusc.2006.11.021
- [18] K. Zhang, M. Wen, G. Cheng, X. Li, Q.N. Meng, J.S. Lian, W.T. Zheng: Vacuum 99 (2014) 233. DOI:10.1016/j.vacuum.2013.05.014
- [19] E.J. Mittemeijer, U. Welzel: Z. Kristallogr. 223 (2008) 552. DOI:10.1524/zkri.2008.1213
- [20] A.D. Zuev: J. Appl. Cryst. 39 (2006) 304. DOI:10.1107/S0021889806005693
- [21] J.G.M. van Berkum, R. Delhez, T.H. De Keijser, E.J. Mittemeijer: Acta Cryst. A52 (1996) 730. DOI:10.1107/S0108767396005727
- [22] P.S. Prevéy: J. Therm. Spray Technol. 9(3) (2000) 369. DOI:10.1361/105996300770349827
- [23] Y.-Y. Chang, D.-Y. Wang, C.-Y. Hung: Surf. Coat. Technol. 200 (2005) 1702. DOI:10.1016/j.surfcoat.2005.08.088
- [24] H.S. Myung, H.M. Lee, L.R. Shaginyan, J.G. Han: Surf. Coat. Technol. 163–164 (2003) 591.
- [25] J. Musil, F. Kunc, H. Zeman, H. Polakova: Surf. Coat. Technol. 154 (2002) 304. DOI:10.1016/S0257-8972(01)01714-5
- [26] M. Sakurai, T. Toihara, M. Wang, W. Kurosaka, S. Miyake: Surf. Coat. Technol. 203 (2008) 171. DOI:10.1016/j.surfcoat.2008.08.060
- [27] N. Panich, W. Vattanaprateep, S. Yong: J. Met. Mater. Miner. 16 (2) (2006) 19.
- [28] J. Stallard, S. Poulat, D.G. Teer: Tribol. Int. 39 (2006) 159. DOI:10.1016/j.triboint.2005.04.011
- [29] H.C. Barshilia, B. Deepthi, K.S. Rajam, K.P. Bhatti, S. Chaudhary: J. Vac. Sci. Technol. A 27 (2009) 29. DOI:10.1116/1.3013858
- [30] H.C. Barshilia, M.S. Prakash, A. Jain, K.S. Rajam: Vacuum 77 (2005) 169. DOI:10.1016/j.vacuum.2004.08.020
- [31] K. Aslantas, I. Ucun, A. Cicek: Wear 274–275 (2012) 442. DOI:10.1016/j.wear.2011.11.010
- [32] A. Devillez, G. Le Coz, S. Dominiak, D. Dudzinski: J. Mater. Process. Technol. 211 (2011) 1590. DOI:10.1016/j.jmatprotec.2011.04.011
- [33] D. Ulutan, T. Ozel: Int. J. Mach. Tools Manuf. 51 (2011) 250. DOI:10.1016/j.ijmachtools.2010.11.003
- [34] M. Gunay, E. Yuclu: Measurement 46 (2013) 913. DOI:10.1016/j.measurement.2012.10.013
- [35] M.A. Shalaby, M.A. El Hakim, M.M. Abdelhameed, J.E. Krzakowski, S.C. Veldhuis, G.K. Dosbaeva: Tribol. Int. 70 (2014) 148. DOI:10.1016/j.triboint.2013.10.011

- [36] D. Zhu, H.D. Xiaoming: *Int. J. Mach. Tools Manuf.* 64 (2013) 60.
DOI:10.1016/j.ijmachtools.2012.08.001
- [37] E. Chiappini, S. Tirelli, P. Albertelli, M. Strano, M. Monno: *Int. J. Mach. Tools Manuf.* 77 (2014) 16.
DOI:10.1016/j.ijmachtools.2013.10.006
- [38] J.L. Cantero, J. Diaz-Aluarez, M.H. Miguelez, N.C. Marin: *Wear* 279 (2013) 885. DOI:10.1016/j.wear.2012.11.004
- [39] R. Suresh, S. Basavarajappa, V.N. Gaitonde, G.L. Samuel: *Int. J. Refract. Met. Hard Mater.* 33 (2012) 75.
DOI:10.1016/j.ijrmhm.2012.02.019
- [40] R. Suresh, S. Basavarajappa, G.L. Samuel: *Measurement* 45 (2012) 1872. DOI:10.1016/j.measurement.2012.03.024

(Received September 1, 2014; accepted November 12, 2014; online since January 27, 2015)

Correspondence address

T. Sampath Kumar
Department of Mechanical Engineering
C. Abdul Hakeem College of Engineering and Technology
Melvisharam
Vellore District – 632509
India
Tel.: +91 4172-267387
Fax: +91 4172-268387
E-mail: sampathpp@gmail.com

Bibliography

DOI 10.3139/146.111190
Int. J. Mater. Res. (formerly Z. Metallkd.)
106 (2015) 4; page 378–390
© Carl Hanser Verlag GmbH & Co. KG
ISSN 1862-5282